Direct measurement of single soft lipid nanotubes: Nanoscale information extracted in a noninvasive manner

Akihisa Yamamoto and Masatoshi Ichikawa*
Department of Physics, Kyoto University, Sakyo, Kyoto 606-8502, Japan
(Received 27 January 2012; revised manuscript received 7 September 2012; published 14 December 2012)

We investigated the dynamics of single soft nanotubes of phospholipids to extract nanoscale information such as the size of the tube, which were several tens to hundreds of nanometers thick. The dynamic properties of the tubes obtained from direct observation by fluorescent microscopy, such as their persistence length, enable us to access the nanoscale characteristics through a simple elastic model of the membrane. The present methodology should be applicable to the nanosized membrane structure in living cells.

DOI: 10.1103/PhysRevE.86.061905 PACS number(s): 87.16.dj, 65.80.−g, 87.14.Cc, 87.15.H−

I. INTRODUCTION

Within organisms, phospholipid membrane is one of the primitive structures working as a compartment wall and a boundary of the cell that can exhibit various topologies and morphologies. While there are too many examples to enumerate, several characteristic morphological activities have been reported in endoplasmic reticulum [1], neurons, and mitochondria [2]. Although the shapes of the membrane as observed in electron micrograph images are fixed or frozen, they must be dynamic in living cells. For example, the adaptive deformation of mitochondria for the environmental changes was recognized [3]. Such dynamic morphologies under nonequilibrium and reactive conditions must have biological significance and should be examined from both biochemical and physicochemical aspects. Toward the issues, a giant vesicle of phospholipids is a useful experimental model to observe a phenomenon or structure of interest under the simplified system.

Giant vesicles which exhibit several tens of micrometers in size have been used as a simple experimental model (e.g., studying their morphological transformation [4], microdomain formation, or lateral phase separation [5]). The encapsulation of biopolymers has been applied for mimicking biochemical functions [6–8] and structures [9,10]. Toxicity by an enzyme on a membrane was probed as a deformation of the vesicle [11]. The affinity of the DNA on a membrane was identified with transcriptional processes [12,13]. A complex system or membrane containing biomolecules was realized in the supported membrane [14]. As mentioned above, recent biophysical approaches that use simple model systems have been shown to be useful for examining such underlying problems on structure and morphology in living systems.

In the present paper, we report a direct observation of single soft nanotubes to yield their nanoscopic characteristics from their dynamics. Dynamical properties, including the diffusion constant, the relaxation time, and the persistence length, are obtained through the use of fluorescent microscopy by use of direct observation methods [15–19]. The combination of a model of membrane elasticity based on the Helfrich scheme [20] with the statics of a fluctuated tube enables us to figure out the thickness of the individual nanotubes below resolution. This strategy would be applicable to nonimmersive *in vivo* measurements within cellular organisms.

II. EXPERIMENTAL METHODS

Phospholipid tubes were made by the natural swelling method [21]. Dioleoyl-L-α-phosphatidylcholine (DOPC, purchased from Wako) and N-(rhodamine red-X)-1,2-dipalmitoyl L-α-phosphatidylethanolamine (Rhodamine-Red DPPE, Avanti Polar Lipids) at a molar ratio of 500 : 1 were dissolved in a chloroform-methanol (=2 : 1) solution, and then dried under a vacuum overnight to form thin lipid films. The dry films were hydrated with 200 μL of distilled water to adjust 0.5 mM, and the solution was incubated at room temperature for 3 hours. The sample was yielded as a mixture of vesicles and tube hollow with unilamellar and multilamella membranes. A tubular shape composed of bilayer membrane could be generated by an adequate composition of lipids [4,22] or during pipetting (i.e., adapting an external force such as shear flow [23,24]). A glass chamber for microscopy observation was made using glass cover slips previously washed with alkaline alcohol. The swelled solution was placed between the slips so that the solution was 2-μm thick, and the chamber was sealed with hydrophobic liquid blocker to prevent evaporation. The sample chamber was set on a fluorescent microscope (Nikon TE2000U). The process of sample loading into the chamber eliminated thicker vesicles and tubes [15]; therefore we can find only the small particles and worm-like chains in the chamber. Since the sample solution was confined within this thin space that was on the order of the focal depth, the shape and motion of the whole chain could be observed as in-focus images. Sequential images were captured by an electron multiplying charge-coupled device (EM-CCD) camera (Hamamatsu Photonics) and recorded at 31.93 frames/s.

Phase diagrams of DOPC suggest the observed chain is not a cylindrical micelle in this condition [25]. Since the present concentration is in an extremely dilute regime where it is far from the cylindrical micelle condition, the dispersed vesicles and tube hollow (including multilamella and unilamellar) can maintain their form in the room temperature. These closed membrane vesicles and tubes are not in a thermodynamically equilibrium phase, but in a stable state (metastable) under the time scale of days. Therefore, the chain would be a tube hollow

*ichi@scphys.kyoto-u.ac.jp

of multilamella and/or a unilamellar membrane. Beside the measurements by the fluorescent observation, we had checked the relative fluorescent intensity to exclude the multilamella tube because stronger fluorescence reflects its multilamella nature. The measured tube hollows which we expected to be unilamellar also exhibited low scatting in darkfield microscopy similar to the unilamellar membrane (giant vesicle) prepared separately.

III. RESULTS

Figure 1(a) shows typical images of the time development of a single phospholipid tube exhibiting translational and intrachain Brownian motion. As shown, we observed individual tubes that were longer than several micrometers and measured their positions and shape. The center of mass $\boldsymbol{r}_{\mathrm{c.m.}}$ of the phospholipid nanotube is calculated as $\boldsymbol{r}_{\mathrm{c.m.}} = \sum_i \boldsymbol{r}_i I(\boldsymbol{r}_i)/\sum_i I(\boldsymbol{r}_i)$, where $I(\boldsymbol{r}_i)$ is the fluorescent intensity of each pixel $\boldsymbol{r}_i$.

The mean square displacement (MSD) of $\boldsymbol{r}_{\mathrm{c.m.}}$ for each tube is shown in Fig. 2(a) as a function of the lag time Δt. From the slopes of MSD in the short time region less than 10 s, the diffusion coefficient D_G is calculated as $\mathrm{MSD} = 4D_G\Delta t + A(\Delta t)^2$, where A is a drift coefficient.

Figure 2(b) shows the MSD of the end points of each tube and the average of scaling indices in the short time region less than 10 s that is determined to be 0.76 ± 0.18.

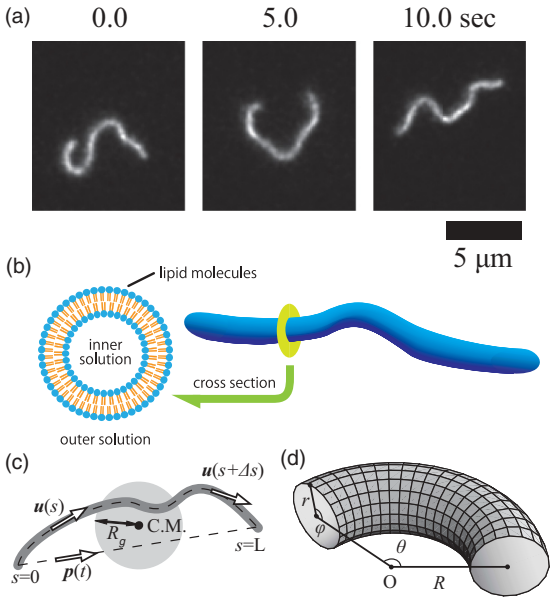

FIG. 1. (Color online) (a) Typical images of a single phospholipid tube in an aqueous solution. The images were taken at intervals of 5.0 s. The scale bar is 5 μm. (b) A schematic illustration of a nanotube. (c) The measured values obtained from image analysis. The radius of gyration R_g is calculated from the spatial distribution of fluorescent intensity; the rotational relaxation time τ_r represents the decay of the correlation of a unit end-to-end vector $\boldsymbol{p}(t)$; the persistence length l_p is defined as the decaying slope of a scalar product of two unit tangent vectors $\boldsymbol{u}(s)$ and $\boldsymbol{u}(s+\Delta s)$. (d) Frame representation of part of a tube. An eel-like tube is assumed to be composed of several sections of tori with various values of R and homogeneous r. Notations used in the calculations are represented as above.

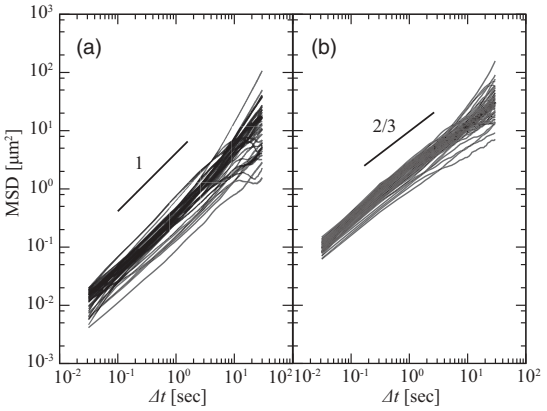

FIG. 2. (a) Log-log plot of measurements of MSD of the center of mass. In the short time region to 10 s, each MSD is proportional to Δt. (b) Log-log plot of MSD of the end points.

The lateral motion of an end point can be predicted by a simple scaling law that the index is calculated to be 2/3 before the configuration undergoes relaxation [26], and thus the experimental results show quite good agreement with the model of polymer dynamics.

As shown in Fig. 1(c), the radius of gyration and the unit end-to-end vector are also obtained as $R_g^2 = \sum_i I(\boldsymbol{r}_i)|\boldsymbol{r}_i - \boldsymbol{r}_{\mathrm{c.m.}}|^2/\sum_i I(\boldsymbol{r}_i)$ and $\boldsymbol{p}(t) = [\boldsymbol{r}_{s=\mathrm{L}}(t) - \boldsymbol{r}_{s=0}(t)]/|\boldsymbol{r}_{s=\mathrm{L}}(t) - \boldsymbol{r}_{s=0}(t)|$, respectively. D_G for each tube is plotted as a function of R_g in Fig. 3(a). The scaling index α of $D_G \propto R_g^{\alpha}$ was $\alpha = -1.3 \pm 0.2$. The rotational relaxation time τ_r of the unit of end-to-end vector $\boldsymbol{p}(t)$ is also obtained in Fig. 3(b) as a function of R_g. The scaling index β for $D_G \propto R_g^{\beta}$ in the experiment was $\beta = 2.9 \pm 0.2$. The relationship of D_G and τ_r is also shown in Fig. 3(c). The scaling index γ for $D_G \propto \tau_r$ was obtained as $\gamma = -3.1$. The superimposed lines in Fig. 3(a), $\alpha = -2$ and $\alpha = -1$, indicate the indices calculated from the Rouse model and Zimm model for polymers, respectively. The indices of $\beta = 4$ and $\gamma = -2$ are the result of the Rouse model, and those of $\beta = 3$ and $\gamma = -3$ are of the Zimm model. These eye guides are the result of indices $D_G \propto N^{-1}$ and $\tau_r \propto N^2$ for Rouse; $D_G \propto N^{-1/2}$ and $\tau_r \propto N^{3/2}$ for Zimm; and $R_g \propto N^{1/2}$ for an ideal chain with a number of segments N [26]. The indices from the present experiment were rather close to those of Zimm.

IV. DISCUSSION

The experiments show that the quasi-two-dimensional chamber enables the observation of the dynamics of the whole contour of the soft nanotubes. Since the yielded dynamics represent or are comparable to previous studies of protein filaments, cylindrical micelles, and so on [27–31], the value of the present result of the lipid tube itself would be reliable, although the chemical and the detailed structures are different. The sample solution within the chamber contains only a tubular structure but not a spherical vesicle. Some kinetic effects such as shear flow and direct contact with glass slips might cause the elimination of the spherical vesicle [23,24].

Next, we discuss and figure out a simple methodology or strategy for determining the unseeable microscopic features of

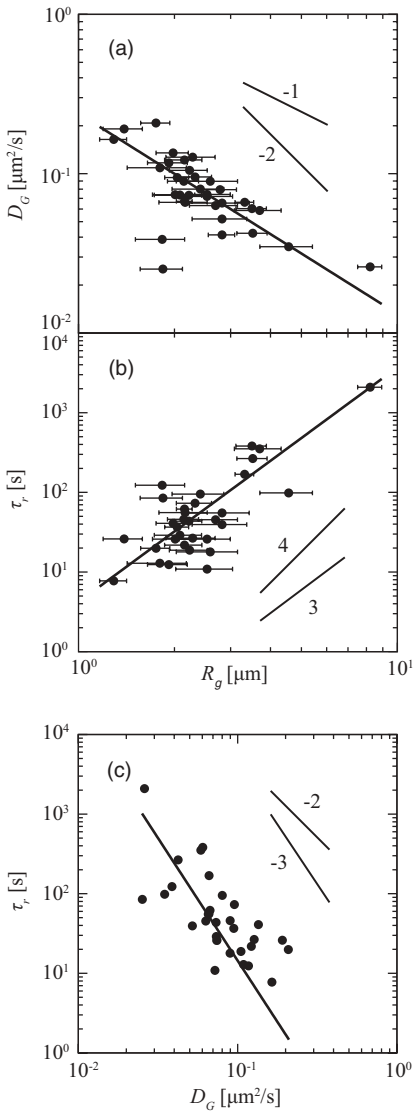

FIG. 3. Relations between (a) the lateral diffusion constant D_G and the radius of gyration R_g, (b) the rotational relaxation time τ_r and R_g, and (c) τ_r and D_G as determined experimentally. Fitting lines are $D_G \propto R_g^{\alpha}$ ($\alpha = -1.3$), $\tau_r \propto R_g^{\beta}$ ($\beta = 2.9$), and $\tau_r \propto D_G^{\gamma}$ ($\gamma = -3.1$), respectively. Superimposed lines show the scaling law from the theory of polymer dynamics; $\alpha = -2$, $\beta = 4$, and $\gamma = -2$ are indices of the Rouse model, and $\alpha = -1$, $\beta = 3$, and $\gamma = -3$ are those of the Zimm model.

the membrane from the observable values by coupling polymer physics and membrane physics through comparing the fluctuation and structural free energy of the tubes. Geometrically, it is easy to assume a bent tube to be comprised of parts of a torus [32], as shown in Fig. 1(d). The bending free energy of the membrane F can be denoted by a Helfrich-type expression as [20]

$$F = \frac{\kappa}{2}\int (C_1 + C_2 - C_0)^2 dA. \tag{1}$$

For part of a torus, C_1 and C_2 are the curvatures that are normal to each other on the membrane surface. C_0 is the spontaneous curvature. For the general case, C_0 is regarded as a nonzero variable. When the small radius and its angle are defined as r and ϕ for the C_1 coordinate, and the large radius and its angle are R and θ for the C_2 coordinate, $C_1 = \frac{1}{r}$ and $C_2 = \frac{\cos\phi}{R + r\cos\phi}$ are given. The area element dA is represented as $dA = r d\phi (R + r\cos\phi) d\theta$. The bending energy of a part of a torus, which is swept in a small angle $\Delta\theta$ by the cross-sectional circle, is written as

$$\begin{aligned}\frac{\Delta F_{\text{torus}}}{\kappa \Delta\theta/2} &= \int \left(\frac{1}{r} + \frac{\cos\phi}{R + r\cos\phi} - C_0\right)^2 r(R + r\cos\phi) d\phi \\ &= \int_0^{2\pi} d\phi \left(b + \frac{\cos\phi}{a + \cos\phi}\right)^2 (a + \cos\phi), \end{aligned} \tag{2}$$

where $a = R/r > 1$ and $b = 1 - C_0 r$. Equation (2) is rewritten as

$$\frac{\Delta F_{\text{torus}}}{\kappa \Delta\theta/2} = \int_0^{2\pi} d\phi \left((b+1)^2 \cos\phi + ab^2 - \frac{a\cos\phi}{a + \cos\phi}\right). \tag{3}$$

The integrals of the first and the second terms in Eq. (3) are 0 and $2\pi a b^2$, respectively. The integral of the third term can be calculated in a complex integration on a unit circle C as

$$\begin{aligned} &-a \oint_C \frac{(z + z^{-1})/2}{a + (z + z^{-1})/2} \frac{dz}{iz} \\ &= -\frac{a}{i} \oint_C \frac{z^2 + 1}{z(z + a - \sqrt{a^2 - 1})(z + a + \sqrt{a^2 - 1})} dz. \end{aligned} \tag{4}$$

This integrand has two simple poles at $z_0 = 0$ and $z_1 = -a + \sqrt{a^2 - 1}$ inside C while $z_2 = -a - \sqrt{a^2 - 1}$ is out from the unit circle. The residues are given as $\text{Res}(z_0) = 1$ and $\text{Res}(z_1) = -a/\sqrt{a^2 - 1}$. We use the residue theorem and then rewrite Eq. (4) as

$$-\frac{a}{i} 2\pi i \sum_{j=0,1} \text{Res}(z_j) = 2\pi \left(\frac{a^2}{\sqrt{a^2 - 1}} - a\right). \tag{5}$$

Therefore, we achieve the following expression from Eq. (2) as

$$\Delta F_{\text{torus}} = \frac{\kappa}{2} \frac{2\pi}{r} \left(\frac{1}{\sqrt{1 - r^2 c^2}} + C_0 r (C_0 r - 2)\right) \Delta s, \tag{6}$$

where c is the curvature of the circular arc drawn by the backbone of the torus and $\Delta s = R\Delta\theta$ corresponds to the small section of the arclength. It should be noted that the term $C_0 r(C_0 r - 2)$ does not include a parameter about the winding of the backbone or curvature c. This term with the spontaneous curvature C_0 just changes the zero point of the free energy. Therefore

$$\Delta F_{\text{torus}} = \frac{\kappa}{2} \frac{2\pi}{r} \frac{1}{\sqrt{1 - r^2 c^2}} \Delta s, \tag{7}$$

is resulted in, not only the case of $C_0 = 0$. It should be reconsidered if the area differential between the inner and outer leaflets is considerable, such as the area-difference elasticity (ADE) model [33]. Now the Taylor series of ΔF_{torus} for c becomes

$$\Delta F_{\text{torus}} = \frac{\kappa\pi}{r} \Delta s + \frac{r\kappa\pi}{2} \Delta s c^2 + \frac{3r^3 \kappa\pi}{8} \Delta s c^4 + \cdots. \tag{8}$$

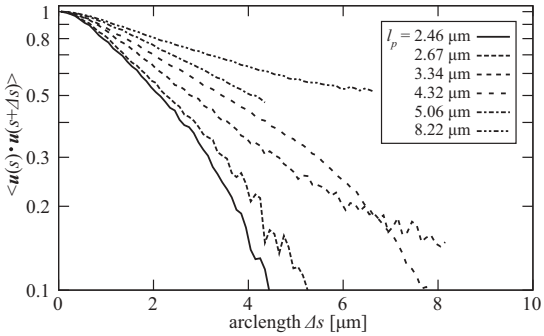

FIG. 4. Typical examples of the correlations of scalar product $\langle \boldsymbol{u}(s) \cdot \boldsymbol{u}(s + \Delta s) \rangle$. The persistence length l_p is determined from the exponential decay in a short region. The correlation at long range and in the vicinity of 0 tends to deviate from exponential fitting.

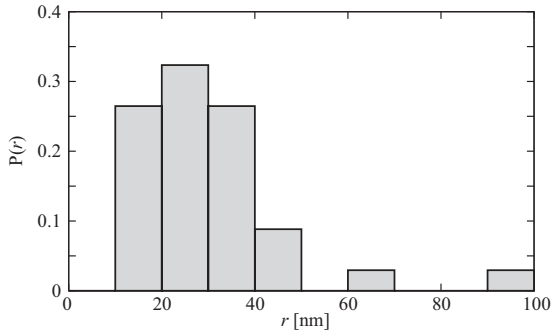

FIG. 5. Distribution of the radii of tubes with $\kappa = 20\ k_B T$.

The first term on the right-hand side represents the bending energy for making a tube from a planar membrane, and the second and later terms are the result of the bending of the backbone and nonlinear terms from the cylinder hollow.

On the other hand, the bending free energy of a chain such as a polymer embedded in two spatial dimensions can be represented as [34,35]

$$\Delta F_{\text{chain}} = \frac{k_B T l_p}{4} \Delta s c^2, \tag{9}$$

where l_p is the persistence length of a chain in two spatial dimensions. If we compare the c^2 terms of Eqs. (8) and (9)

$$\kappa = \frac{k_B T l_p}{2\pi r} \tag{10}$$

is obtained as a first approximation. Since this form is applicable to not only $C_0 = 0$ but $C_0 \neq 0$ conditions, it would be useful to treat the situation of a protein binding membrane [36].

The persistence length l_p of a nanotube can be obtained from the experiments as

$$\langle \boldsymbol{u}(s) \cdot \boldsymbol{u}(s + \Delta s) \rangle = \exp\left(-\frac{\Delta s}{l_p}\right), \tag{11}$$

where $\boldsymbol{u}(s)$ is a two-dimensional unit tangent vector at which s is the path length along the backbone from one end, as shown in Fig. 1(c). The value of l_p for each tube can be estimated from the slope in Fig. 4. The short-range correlation lower than 0.5 μm is excluded from the fitting analysis [37,38]. The above equation includes an approximation which adapts the present geometry, confinement thickness of the solution Δz, and the persistence length l_p (i.e., the persistence length calculated from the two-dimensional projection image of the polymer chain within a quasi-two-dimensional space) asymptotically converges to the actual two-dimensional persistence length [39]. The present experimental values, thickness of the confining space, and the order of magnitude of the persistence length satisfy the above approximation.

The bending rigidity of a DOPC bilayer membrane has been experimentally measured by various methods, such as the pipette aspiration method [40], the electrodeformation method [41], x-ray scattering [42], and volumetric measurement [43]. These studies point out the value is 18 to 27 $k_B T$, or approximately 20 $k_B T$. Therefore, the thickness of each nanotube can be calculated from Eq. (10) by substituting the value into κ, and the result is shown in Fig. 5. The radii of the nanotubes, which are evaluated individually, are distributed around 30 nm. This value is consistent with the microscopy observation, considering the limitations due to the resolution and diffraction limit, where the thickness is less than or equal to the fluorescent blurring length. In this manner, the dynamical analysis of the micrometer-scale behaviors has revealed the size of a nanostructure.

The radii of the tubes can be estimated through another approach by considering the tube as a polymer chain divided into $N = L/b$ segments, where L is the contour length and $b = 2l_p$ is the Kuhn length. The diffusion constant of a rod with length b and radius r in two spatial dimensions D_S is calculated as [26]

$$D_S = \frac{3}{8} \frac{k_B T \ln(b/2r)}{\pi \eta_s b}, \tag{12}$$

where η_s is the viscosity of bulk water. D_S can also be represented as $D_S = N D_G = L D_G / b$ in the Rouse model. Although the compensations for the entire length of the tube and the increase in viscosity from the walls are considerable [44], a simple expression in terms of r can be obtained as

$$\frac{l_p}{r} = \exp\left(\frac{8\pi \eta_s}{3 k_B T} L D_G\right). \tag{13}$$

Since only L and D_G are indefinite but experimentally observable variables, both r and the bending modulus κ of the membrane can be estimated from Eqs. (10) and (13). However, the calculated values of r obtained from Eq. (13) were scattered due to the exponential term, and the form is too sensitive to evaluate r and κ here.

The above discussion enables us to extract information regarding nanometer-scale properties of individual tubes from the dynamics of respective ones, such as the size and bending modulus. Generally, diffraction limitations or the fluorescent blurring of approximately 200 nm in length hides nanoscopic structures from optical microscopy. Actually, cylindrical micelles composed of various amphipathic molecules several nanometers thick were visualized as thicker filaments [15–19]. Based solely on a spatial analysis, the apparent sizes of such worm-like micelles in the fluorescent images were close to around 500 nm in diameter. But this would not become so a large problem for the cylindrical worm-like micelles because

the thicknesses are first defined by the molecular nature of the amphiphiles and separately identified by electron micrographs [45–47]. The characteristics of micelles in ensemble can be also measured by scattering experiments [48,49]. However, this optical limitation would become crucial for the tubes since the thickness of the tubular vesicle is varied and adapted by the amounts of surface area and volume of the vesicle. The present method can access the nanosized tube that is one order of magnitude smaller than the length of optical resolution. This would be advantageous in real-time measurements of living cells compared to the electron microscopy, which have thus far been used to measure nanosized structures [45,50]. Living cells and nonequilibrium situations require nonimmersive approaches for real-time measurements, where fluorescence or optical microscopies exhibit moderate damage on live cells rather than the electron microscopy at this time. Although alkyl chains of the palmitoyl-group of DPPE raise the bending rigidity of the membrane compared to the homogeneous DOPC membrane and the effect of the rhodamine on the ethanol amine is complex, the fraction of Rho-DPPE is quite low so that we can regard its effect as essentially negligible.

The present strategy is also applicable to measure the bending rigidity of the membrane inversely by use of separately measured values about the thickness of the tubes. For example, F-BAR protein families which are expected to induce budding or tube-generating transition in a living cell also make a spherical vesicle into tubules *in vitro* model experiment. Since the radius of the tube is regulated by the protein structure, the reinforced effect by the proteins have been yielded quantitatively as a time-development behavior [36]. It is known that bending rigidity of the membrane can be measured by optical tweezers, a tiny needle, or micropipette [40,51–53], but it can be difficult to use with an internal structure confined in a living cell. On the other hand, the present method is free from adhesive manipulations and modifications and the model itself can be applicable to the three-dimensional conformation of the tube. Contemplating for the characteristics of the methodologies, future developments of three-dimensional tomographic imaging technique will give the obvious advantages to the image analysis method including the present approach.

Although the model described here is constructed under the approximation of an elastic membrane, future work should consider the implications of the fact that a bilayer membrane is a liquid membrane. First, there is friction between the membrane and solution. This friction is discussed in plane geometry [54], but internal friction within the tube is more difficult to consider due to the coupling of the shape of the tube vesicle. Another important consideration is thickness uniformity. The bent tube in this analysis is assumed to have a uniform thickness that does not depend on the backbone curvature c. However, the bending energy is also a function of the tube radius r, and not only c, as in the bending form of Eq. (7) or (8). r has a strong effect in higher-order terms. Nonlinear elastic behavior of this type is sometimes observed in experiments, and it would be interesting to quantify. These factors may affect those on a larger scale [i.e., those in Eqs. (11) and (12)]. Hydrodynamics should be also considered for a future work. Hydrodynamic interaction through the membrane and that through the inner part of the tube may be effective to the dynamics, but it is now an open question. These nonlinearity of single chains might complement the rheology on a macroscopic scale as in a worm-like micelle solution [55].

V. CONCLUSION

In conclusion, the direct observation enables to analyze the dynamics of single phospholipid soft nanotubes. We have described a method for estimating the thickness and rigidity of a phospholipid nanotube from the observed Brownian motion. The ability to avoid damaging the sample object should be useful not only for measuring the dynamical response of a membrane under nonequilibrium conditions but also for revealing the membrane properties of organelles such as mitochondria and endoplasmic reticulum.

ACKNOWLEDGMENTS

We acknowledge Professor K. Yoshikawa for his helpful discussion, and Dr. M. Hörning and Dr. Y. Maeda for a critical reading of the manuscript. We also thank Dr. A. Isomura and Dr. T. Yamanaka for their help with analysis. This work was supported by iCeMS Cross-Disciplinary Research Promotion Project, by the JSPS Core-to-Core Program "International research network for non-equilibrium dynamics of soft matter" and by the grant-in-aid for the Grobal COE Program "The Next Generation of Physics, Spun from Universality and Emergence" from the Ministry of Education, Culture, Sports, Science, and Technology (MEXT) of Japan.

APPENDIX: CONFINE EFFECTS ON APPARENT LENGTH AND ON VISCOSITY

Here we discuss additional effects on the apparent length of the tube and on the viscosity in the quasi-two-dimensional space.

The apparent contour length L_2 is a projection of the actual contour length L. For simplicity, a single wave approximation is applied for the present geometry as

$$z(s) = \frac{\Delta z}{2} \sin\left(\frac{2\pi}{\lambda} s\right), \quad (0 \leqslant s \leqslant L_2). \tag{A1}$$

This z-axial undulation $z(s)$ can be assumed to be independent on the shape of the tube in the xy plane. The effective thickness Δz is approximated as $\Delta z = 1\ \mu$m because the entire image of a tube is clearly seen during observation. Wavelength λ is approximated as $\lambda = 2b$, where b is the Kuhn length. Thus, L can be represented as

$$L = \int_0^{L_2} ds \sqrt{1 + \left(\frac{\Delta z}{2} \frac{\pi}{2l_p}\right)^2 \cos^2\left(\frac{\pi}{2l_p} s\right)}. \tag{A2}$$

In this expression, L exhibits 1.0 to 1.1 times longer than L_2 obtained from the projected image.

On the other hand, the increased viscosity between two nearby walls should be considered. This effect was discussed previously [44] and is approximated to apply to the present geometry as

$$\eta_s(r) = \frac{\eta_{s0}}{1 - \frac{9}{16}\left(\frac{r}{z} + \frac{r}{d-z}\right)}, \tag{A3}$$

where η_{s0}, d, and z are the viscosity of bulk water, distance between two flat walls, and the average distance from the wall, respectively. Substituting Eq. (A3) into η_s of Eq. (13), the equation becomes nonlinear about r. Numerical estimation results $\eta_s(r)$ is 1.0 to 1.1 times larger than the η_{s0} which is without wall effect. The effect on viscosity from the walls can be negligible under the present qualitative treatment.

[1] I. A. Sparkes, L. Frigerio, N. Tolley, and C. Hawes, Biochem. J. **423**, 145 (2009).
[2] P. J. Lea, R. J. Temkin, K. B. Freeman, G. A. Mitchell, and B. H. Robinson, Microsc. Res. Tech. **27**, 269 (1994).
[3] J. Bereiter-Hahn and M. Vöth, Microsc. Res. Tech. **27**, 198 (1994).
[4] H. Hotani, F. Nomura, and Y. Suzuki, Curr. Opin. Colloid Interface Sci. **4**, 358 (1999).
[5] S. L. Veatch and S. L. Keller, Biochim. Biophys. Acta **1746**, 172 (2005).
[6] P. Walde, K. Cosentino, H. Engel, and P. Stano, ChemBioChem **11**, 848 (2010).
[7] K. Tsumoto, S.-I. M. Nomura, Y. Nakatani, and K. Yoshikawa, Langmuir **17**, 7225 (2001).
[8] S.-I. M. Nomura, K. Tsumoto, T. Hamada, K. Akiyoshi, Y. Nakatani, and K. Yoshikawa, ChemBioChem **4**, 1172 (2003).
[9] M. Hase and K. Yoshikawa, J. Chem. Phys. **124**, 104903 (2006).
[10] M. Negishi, M. Ichikawa, M. Nakajima, M. Kojima, T. Fukuda, and K. Yoshikawa, Phys. Rev. E **83**, 061921 (2011).
[11] R. Wick, M. I. Angelova, P. Walde, and P. L. Luisi, Chem. Biol. **3**, 105 (1996).
[12] A. Kato, E. Shindo, T. Sakaue, A. Tsuji, and K. Yoshikawa, Biophys. J. **97**, 1678 (2009).
[13] A. Tsuji and K. Yoshikawa, J. Am. Chem. Soc. **132**, 12464 (2010).
[14] M. Tanaka and E. Sackmann, Nature (London) **437**, 656 (2005).
[15] K. Rajagopal, A. Mahmud, D. A. Christian, J. D. Pajerowski, A. E. X. Brown, S. M. Loverde, and D. E. Discher, Macromolecules **43**, 9736 (2010).
[16] P. A. Stone, S. D. Hudson, P. Dalhaimer, D. E. Discher, E. J. Amis, and K. B. Migler, Macromolecules **39**, 7144 (2006).
[17] Y. Geng, P. Dalhaimer, S. Cai, R. Tsai, M. Tewari, T. Minko, and D. E. Discher, Nat. Nanotech. **2**, 249 (2007).
[18] S. M. Loverde, D. A. Pantano, D. A. Christian, A. Mahmud, M. L. Klein, and D. E. Discher, Curr. Opin. Solid State and Materials Sci. **15**, 277 (2011).
[19] S. Cai, K. Vijayan, D. Cheng, E. M. Lima, and D. E. Discher, Pharm. Res. **24**, 2099 (2007).
[20] W. Helfrich, Z. Naturforsch. **28c**, 693 (1973).
[21] D. D. Lasic, Biochem. J. **256**, 1 (1988).
[22] S. M. Nomura, Y. Mizutani, K. Kurita, A. Watanabe, and K. Akiyoshi, Biochim. Biophys. Acta. **164**, 1669 (2005).
[23] O. Rossier, D. Cuvelier, N. Borghi, P. H. Puech, I. Derényi, A. Buguin, P. Nassoy, and F. Brochard-Wyart, Langmuir **19**, 575 (2003).
[24] V. Kantsler, E. Segre, and V. Steinberg, Phys. Rev. Lett. **101**, 048101 (2008).
[25] B. A. Bergenståbl and P. Stenius, J. Phys. Chem. **91**, 5944 (1987).
[26] M. Doi and S. F. Edwards, *The Theory of Polymer Dynamics* (Oxford University Press, New York, 1988).
[27] E. Barry, D. Beller, and Z. Dogic, Soft Matter **5**, 2563 (2009).
[28] J. Käs, H. Strey, J. X. Tang, D. Finger, R. Ezzell, E. Sackmann, and P. A. Janmey, Biophys. J. **70**, 609 (1996).
[29] L. Le Goff, O. Hallatschek, E. Frey, and F. Amblard, Phys. Rev. Lett. **89**, 258101 (2002).
[30] Y. Han, A. M. Alsayed, M. Nobili, J. Zhang, T. C. Lubensky, and A. G. Yodh, Science **314**, 626 (2006).
[31] P. Dalhaimer, F. S. Bates, and D. E. Discher, Macromolecules **36**, 6873 (2003).
[32] U. Seifert, Phys. Rev. Lett. **66**, 2404 (1991).
[33] U. Seifert, Adv. Phys. **46**, 13 (1997).
[34] L. D. Landau and E. M. Lifshitz, *Statistical Physics, 3rd Ed., Course of Theoretical Physics, Vol. 5* (Pergamon, New York, 1994).
[35] P. Gutjahr, R. Lipowsky, and J. Kierfeld, Europhys. Lett. **76**, 994 (2006).
[36] Y. Tanaka-Takiguchi *et al.*, Langmuir (in press), doi: 10.1021/la303902q.
[37] A. Ott, M. Magnasco, A. Simon, and A. Libchaber, Phys. Rev. E **48**, R1642 (1993).
[38] Z. Dogic, J. Zhang, A. W. C. Lau, H. Aranda-Espinoza, P. Dalhaimer, D. E. Discher, P. A. Janmey, R. D. Kamien, T. C. Lubensky, and A. G. Yodh, Phys. Rev. Lett. **92**, 125503 (2004).
[39] J. Hendricks, T. Kawakatsu, K. Kawasaki, and W. Zimmermann, Phys. Rev. E **51**, 2658 (1995).
[40] W. Rawicz, K. C. Olbrich, T. McIntosh, D. Needham, and E. Evans, Biophys. J. **79**, 328 (2000).
[41] R. S. Gracia, N. Bezlyepkina, R. L. Knorr, R. Lipowsky, and R. Dimova, Soft Matter **6**, 1472 (2010).
[42] Y. Lyatskaya, Y. Liu, S. Tristram-Nagle, J. Katsaras, and J. F. Nagle, Phys. Rev. E **63**, 011907 (2000).
[43] N. Kučerka, S. Tristram-Nagle, and J. F. Nagle, J. Membrane Biol. **208**, 193 (2005).
[44] B. Lin, J. Yu, and S. A. Rice, Phys. Rev. E **62**, 3909 (2000).
[45] J. Grumelard, A. Taubert, and W. Meier, Chem. Commun. **2004**, 1462 (2004).
[46] P. Dalhaimer, H. Bermudez, and D. E. Discher, J. Polym. Sci. B. Polym. Phys. **42**, 168 (2004).
[47] E. A. Simone, T. D. Dziubla, D. E. Discher, and V. R. Muzykantov, Biomacromolecules **10**, 1324 (2009).
[48] B. Lonetti, A. Tsigkri, P. R. Lang, J. Stellbrink, L. Willner, J. Kohlbrecher, and M. P. Lattinga, Macromolecules **44**, 3583 (2011).
[49] G. V. Jensen, Q. Shi, G. R. Deen, K. Almdal, and J. S. Pedersen, Macromolecules **45**, 430 (2012).
[50] T. Imae, K. Funayama, M. P. Krafft, F. Giulieri, T. Tada, and T. Matsumoto, J. Colloid Interf. Sci. **212**, 330 (1999).
[51] L. Bo and R. E. Waugh, Biophys. J. **55**, 509 (1989).
[52] M. Ichikawa and K. Yoshikawa, Appl. Phys. Lett. **79**, 4598 (2001).
[53] Y. Shitamichi, M. Ichikawa, and Y. Kimura, Chem. Phys. Lett. **479**, 274 (2009).
[54] S. Ramachandran and S. Komura, J. Phys.: Condens. Matter **23**, 072205 (2011).
[55] R. W. Mair and P. T. Callaghan, Europhys. Lett. **36**, 719 (1996).